Marine and Petroleum Geology 139 (2022) 105575

Contents lists available at ScienceDirect

Marine and Petroleum Geology

journal homepage: www.elsevier.com/locate/marpetgeo

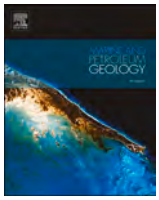

Deep and shallow gas occurrence in the NW Sicilian Channel and related features

Giulia Matilde Ferrante *, Flavio Accaino, Dario Civile, Emanuele Lodolo, Valentina Volpi, Roberto Romeo, Daniela Accettella

Istituto Nazionale di Oceanografia e di Geofisica Sperimentale - OGS, Trieste, Italy

ARTICLE INFO

Keywords:
Sicilian Channel
High-resolution and multi-channel seismic profiles
Pockmarks
Mud-volcanoes
Phase inversion
Tomographic inversion
AVO analysis
Thermogenic gas

ABSTRACT

In this paper we present a combined analysis of recent swath bathymetric data, very high-resolution seismic and multi-channel seismic profiles, integrated with a vintage crustal seismic profile, acquired in the NW Sicilian Channel (Central Mediterranean Sea). These data have been analyzed with the main aim of studying the gas presence and related features in both the subsurface and at the seafloor, through the recognition of amplitude and velocity anomalies in the entire Miocene-Pleistocene sedimentary succession. Our results shed light on the possible gas origin and migration mechanisms. In particular, we support the hypothesis of a gas derivation by thermal cracking of organic matter and suggest the shaly/marly intercalations hosted in the Meso-Cenozoic carbonate succession as a possible source rock. Deep lithospheric faults systems and associated fractures provide preferential paths for gas migration and accumulation in the Miocene-Quaternary sandy and carbonate layers. Gas is then able to locally reach the seafloor originating positive (mud volcanoes) and negative (pockmarks) morphologies.

1. Introduction

Understanding the mechanisms of fluid flow and accumulation in the subsurface is crucial for hydrocarbon exploration purposes as well as for the hazard assessment related to fluid presence and expulsion, which can be associated with a remobilization of unconsolidated sediments (Hovland et al., 1985; Davis, 1992). Moreover, there is a growing interest both in the identification and characterization of free gas in shallow marine sediments and in understanding its degassing mechanisms, which play an increasingly important role in global studies on climate change. In fact methane, the predominant biogenic gas in marine sediments, is considered one of the most important greenhouse contributors (Judd and Hovland, 1992; Hovland et al., 1993; Judd et al., 1997). The presence of gas in marine sediments is testified by various markers, such as signal amplitude and/or velocity anomalies on seismic data and morphological features on the seabed. These pieces of evidence document that gas has migrated and may still be migrating through the seafloor (Judd and Hovland, 1992). Local enhanced reflections with polarity reversals (bright spots) along specific horizons can testify to the lateral propagation and accumulation, whereas acoustic turbidity and blanking may result from the adsorption of acoustic energy in the overlying gas-charged sediments (Judd and Hovland, 1992; Schroot Schuttenhelm, 2003; Donda et al., 2015), preventing signal penetration. Such signatures, however, can also be the result of large changes in acoustic impedance between adjacent media, without involving any gas presence. For example, interbedding of lignite, coal or gravel in soft sediments can produce effects similar to bright spots (Judd and Hovland, 1992). In order to reduce this uncertainty, it is common practice to look for various characteristics of gas-bearing sediments, notably a reduction in P-wave velocity, and to perform amplitude variation with angle/offset (AVA/AVO) analysis. Vertical fluid-flow related features in seismic data are generally represented by pipes and chimneys, i.e. vertical or sub-vertical cone-shaped anomalies characterized by discontinuous or chaotic reflections that interrupt the continuity of the sedimentary succession, sometimes up to the seafloor (Cartwright et al., 2007; Løseth et al., 2009). In this case, bathymetric data are essential to identify and characterize the seafloor expression of such seepages, which may control the formation of both positive (carbonate mounds and mud volcanoes) or negative (pockmarks) morphologies (Judd et al., 2002; Etiope, 2015). The generated structure depends on a variety of parameters, e.g. the source of fluid, the flow type, the structural setting and the nature of the hosting sediment (Cartwright et al., 2007; Huuse

* Corresponding author.
E-mail address: gmatildeferrante@gmail.com (G.M. Ferrante).

https://doi.org/10.1016/j.marpetgeo.2022.105575
Received 13 September 2021; Received in revised form 3 December 2021; Accepted 3 February 2022
Available online 9 February 2022

et al., 2010).

This work investigates the presence of gas in the north-western part of the Sicilian Channel (SC) and, in particular, in the Capo Granitola-Sciacca offshore sector, within ~25 km from the Sicilian coast (Figs. 1 and 2). The SC is a wide foreland area considered one of the most productive hydrocarbon provinces of the Mediterranean Sea (Casero, 2004; Granath and Casero, 2004; Fink and Zimmer, 2012). In particular, the eastern sector of the SC has been intensively explored in the past decades with significant oil and gas discoveries (e.g. the Vega Field, the largest single oil field in the Mediterranean Sea, located between the south-eastern coast of Sicily and the Island of Malta, see Fig. 1 for location), and the recognition of both microbial and thermogenic fluid flow systems across a wide depth range (Savini et al., 2009; Micallef et al., 2011; Taviani et al., 2013). Instead, the north-western sector of the SC is relatively poorly known, except for the Mazara del Vallo-Sciacca offshore, in which the Nilde oil field has been identified (see Fig. 1 for location). The reservoir is hosted in Langhian-Serravallian carbonates, called Nilde Formation (Fm.) within a thrust-related anticlinal structural trap (Riva et al., 2017). In other places, the presence of fluids on the seafloor has been potentially associated with magmatism, such as those documented in the Pantelleria Island (Parello et al., 2000) and at the Graham Bank (Coltelli et al., 2016; Spatola et al., 2018).

The aims of the present study are: i) to document the presence of gas in the Miocene-Quaternary succession; ii) to understand the mechanisms of its migration, analyzing the different types of seafloor manifestations (pockmarks, mud volcanoes, gas flares) and their distribution; iii) to hypothesize the possible sources of gas in the study area. For these purposes, geophysical data at different resolutions (multi-channel seismic reflection data, very high-resolution sub-bottom profiles and bathymetric data) were integrated with the information from the nearby boreholes and the literature on the geology of the area. A tomographic approach was used to identify velocity anomalies and an AVA analysis was performed to recognize the top of gas-bearing formations. Furthermore, seismic attributes were calculated to provide additional evidence for the presence of gas in the sediments.

2. Geological setting

The study area is located in the north-western part of the SC, a wide shallow-water area located between Tunisia and Sicily (Fig. 1). The SC represents the northern part of the African continental plate and its tectonic setting is the product of two independent geodynamic processes (e.g., Jongsma et al., 1985; Boccaletti et al., 1987; Reuther et al., 1993; Corti et al., 2006; Argnani, 2009; Civile et al., 2010, 2018, 2021): in the northern part, the building of the Sicilian-Maghrebian thrust belt (Fig. 1), generated by the NNW-oriented Neogene convergence between African and European plates (Gueguen et al., 1998; Goes et al., 2004; Carminati et al., 2012); in the central part, the Pliocene-Quaternary rift-related processes that produced the three NW-trending deep grabens of Pantelleria, Linosa and Malta (Fig. 1). These two tectonic domains are crossed by the Capo Granitola-Sciacca Fault Zone (CGSFZ) (Civile et al., 2018), a NNE-oriented, lithospheric shear zone extended for at least 200 km from the Linosa Island to the Capo Granitola-Sciacca coast of Sicily (Fig. 1). It mainly developed since Early Pliocene and it is currently characterized by a left-lateral kinematics (Argnani, 1990; Argnani et al., 1986; Antonelli et al., 1988; Finetti and Del Ben, 2005;

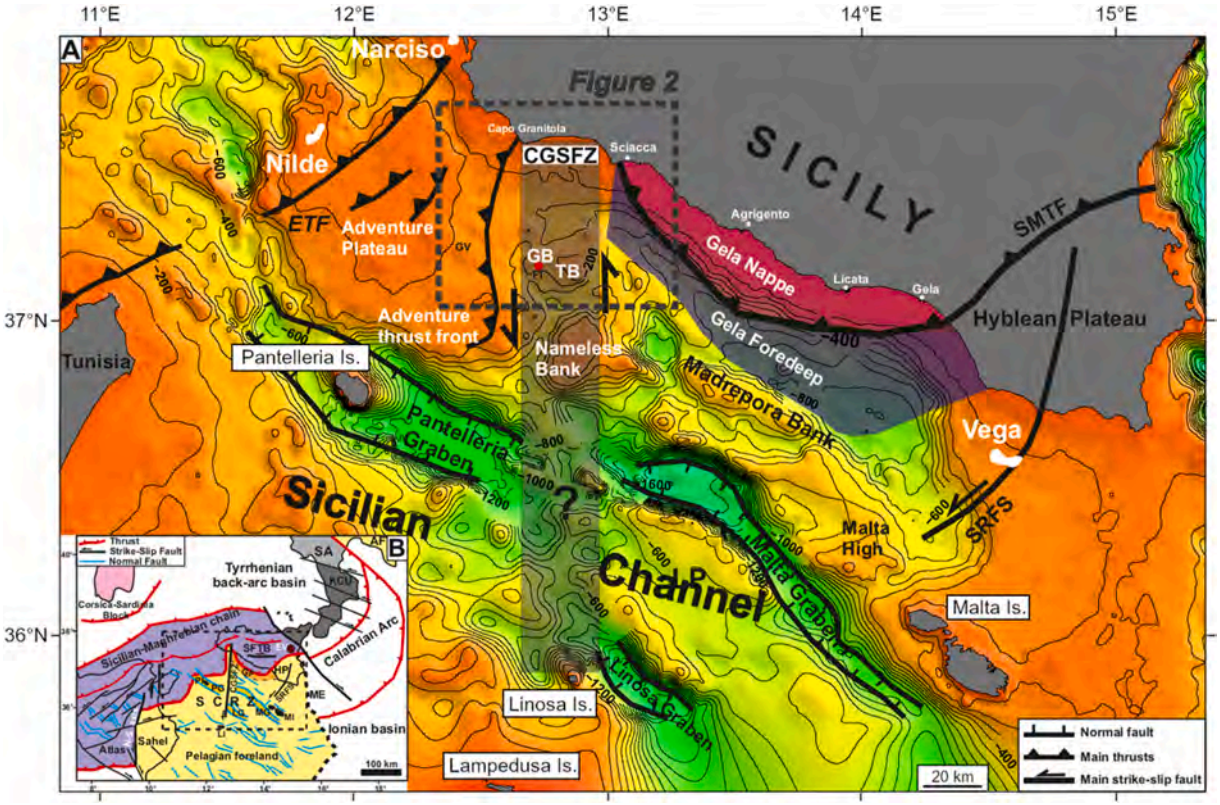

Fig. 1. A) Simplified structural and physiographic map of the Sicilian Channel. Bathymetric data are derived from EMODnet Digital Terrain Model (http://www.emodnet-bathymetry.eu/). The position of the hydrocarbon fields cited in the paper is also reported (Narciso, Nilde and Vega). The dotted rectangle is the area shown in Fig. 2. B) Main geodynamic features of the Central Mediterranean area. The dotted rectangle is the area reported in Fig. 1A. Abbreviations: AF, Apulian foreland; CGSFZ, Capo Granitola-Sciacca Fault Zone; ETF: Egadi Thrust Front; EV, Etna Volcano; FI, Ferdinandea Island; GB: Graham Bank; GF, Gela foredeep; KCU, Kabilo-Calabride tectonic units; LG, Linosa Graben; LI, Linosa Island; ME, Malta Escarpment; MI, Maltese Islands; MG, Malta Graben; PI, Pantelleria Island; PG, Pantelleria Graben; SA, Southern Apennines; SCRZ, Sicilian Channel Rift Zone; SFTB, Sicilian Fold and Thrust Belt, SMTF: Sicilian-Maghrebian Chain Frontal Thrust; SRFS: Scicli-Ragusa Fault System TB: Terrible Bank.

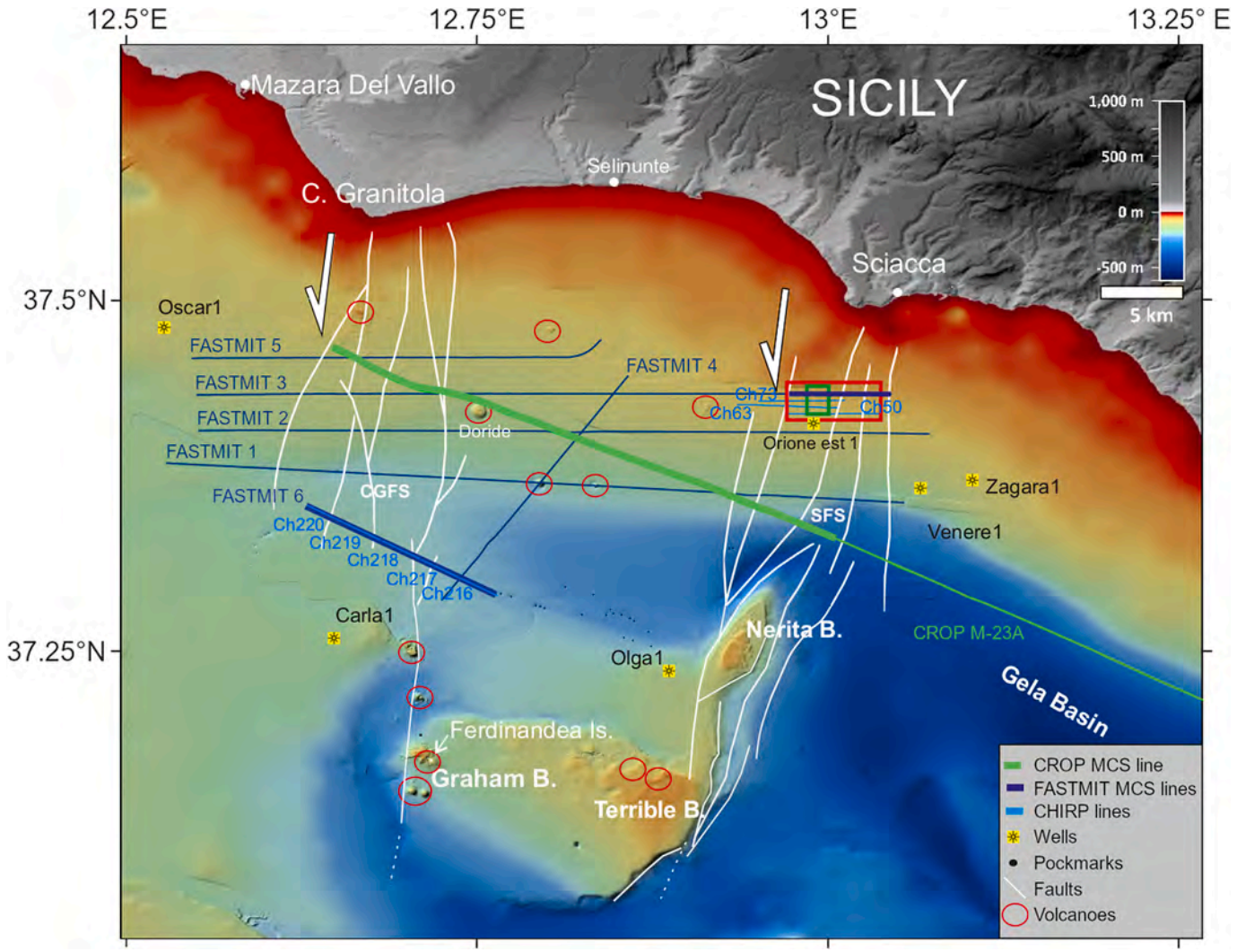

Fig. 2. Detailed bathymetric map of the NW Sicilian Channel (location in Fig. 1) showing the position of the main tectonic lineaments associated with the CGSFZ, volcanic edifices and pockmarks. The location of the available hydrocarbon wells is also reported. The FASTMIT multi-channel seismic lines are shown in dark blue, the CROP M-23 A multi-channel seismic line is in green. The bold lines represent the multi-channel seismic profiles presented in this study, whereas the analyzed CHIRP profiles are in light blue (see text for explanation). The green box corresponds to Fig. 12, whereas the red box corresponds to Fig. 13. Abbreviations: CGFS, Granitola Fault System; SFS, Sciacca Fault System. (For interpretation of the references to colour in this figure legend, the reader is referred to the Web version of this article.)

Ghisetti et al., 2009; Calò and Parisi, 2014; Soumaya et al., 2015; Fedorik et al., 2018; Civile et al., 2018, 2021; Ferranti et al., 2019; Palano et al., 2020). On the basis of seismological and geophysical evidence, Calò and Parisi (2014) supposed that the CGSFZ is a sub-vertical lithospheric shear zone affecting the crust and the upper mantle down to at least 70 km. A significant seismicity is recorded along the CGSFZ (Calò and Parisi, 2014; Coltelli et al., 2016; Palano et al., 2020), although in some regions it is lacking, where either local heating or highly fractured units are thought to affect the elastic parameters of the lower crust, somehow accommodating the stress (Calò, 2013; Calò and Parisi, 2014). One of these zones corresponds to the study area (Figs. 1 and 2), which lies between the Sicily coast and the Graham and Terrible banks. This area includes the northern part of the CGSFZ, consisting of two fault systems: the Capo Granitola Fault System to the west (CGFS) and the Sciacca Fault System (SFS) to the east (Fig. 2). These are both characterized by the presence of positive flower structures (Fedorik et al., 2018; Civile et al., 2018; Ferranti et al., 2019) generated by tectonic inversion of NNE-oriented Late Miocene normal faults (Civile et al., 2018). Evidence of Quaternary tectonic activity is documented along these two fault systems (Civile et al., 2018; Ferranti et al., 2019), whereas the zone between the two fault systems shows a negligible Pliocene-Quaternary tectonic deformation, except for the Terrible Bank, which is affected by WNW to NW-trending sub-vertical normal faults (Civile et al., 2018). Furthermore, the area of study is characterized by scattered Quaternary submarine magmatism which mostly produced small monogenic edifices, recognized on the Graham and Terrible Banks and in the nearshore of Capo Granitola-Sciacca coast of Sicily (Coltelli et al., 2016; Lodolo et al., 2019; Cavallaro and Coltelli, 2019, Fig. 2). The most famous volcanic manifestation is the remnant of the ephemeral Ferdinandea Island (Fig. 2), generated by a surtseyan-type eruption occurred in 1831 on the Graham Bank (Washington, 1909; Colantoni et al., 1975). The origin of the magmatism in this area has been related to the rising of magmas along the lithospheric faults of the CGSFZ (Civile et al., 2018).

The sedimentary succession of the area is reconstructed on the basis of the literature information (Di Stefano et al., 1993; Catalano et al., 1993; Ghisetti et al., 2009; Cavallaro et al., 2017; Civile et al., 2014, 2018; Ferranti et al., 2019) and the available well data (Fig. 2). Fig. 3 shows the succession of the Carla 1 borehole, located close to the FASTMIT 6 seismic line analyzed in this study. It consists of a

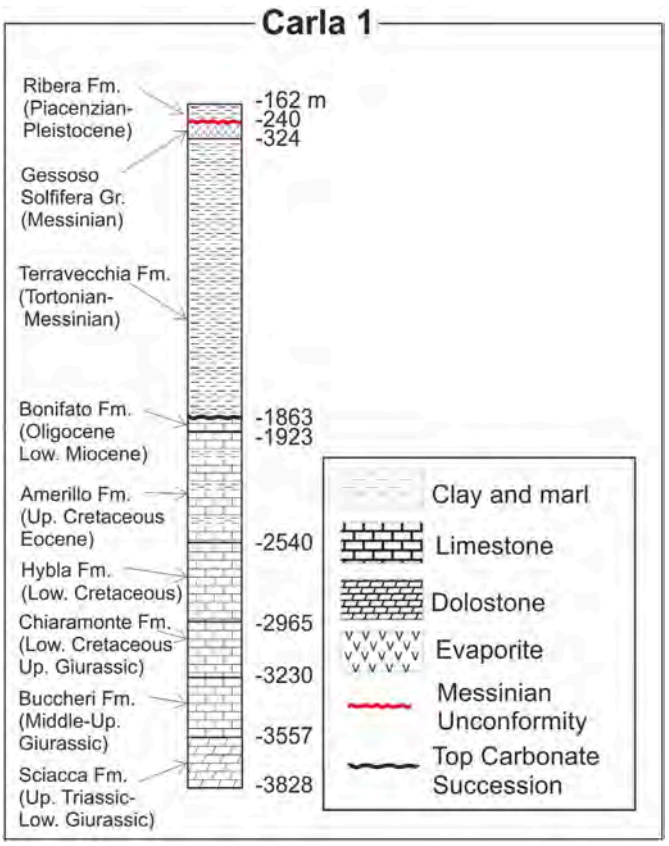

Fig. 3. Simplified stratigraphic column of Carla1 well (see Fig. 2 for location), which is representative of the sedimentary succession of the study area.

Triassic-Middle Miocene carbonate succession overlain by shelf siliciclastic deposits of the Tortonian-Lower Messinian Terravecchia Fm., characterized, in the area, by strong thickness variations from about 250 m to over 1500 m (Civile et al., 2018). Locally, Messinian evaporites and related sediments of the Gessoso-Solfifera Group, formed by some tens of meters of gypsum with thin marly and clayey intercalations, can be present. The lower part of the Pliocene-Quaternary succession, lying on the Messinian Unconformity, is composed of pelagic marls and marly limestones of the Zanclean Trubi Fm., which is covered by Piacenzian-Pleistocene shelf clayey deposits with sandy intercalations of the Ribera Fm. These two formations are not recognizable in the Carla 1 well but have been found in other nearby boreholes (see Civile et al., 2014, 2018).

3. Data

The geophysical dataset analyzed in this work have been acquired in the framework of the FASTMIT (*FAglie Sismogeniche e Tsunamigeniche nei Mari ITaliani*) project, coordinated by the Istituto Nazionale di Oceanografia e di Geofisica Sperimentale (OGS) and funded by the Italian Ministry of University and Research (MIUR). The FASTMIT project was aimed at studying the two fault systems of Capo Granitola and Sciacca and at investigating their seismogenic potential. In particular, six multi-channel seismic (MCS) reflection lines, bathymetric and magnetic data, and very high-resolution sub-bottom profiles (CHIRP) were acquired by the R/V *OGS Explora* in 2017 and 2018 (Fig. 2). Eight CHIRP profiles, the MCS line FASTMIT 6 and part of the MCS line FASTMIT 3 are analyzed in this study (Fig. 2). Furthermore, this dataset was integrated by a part of the vintage MCS line CROP M-23 A, acquired in the 1990s in the framework of the Italian Deep Crust Project, which has been completely re-processed. The acquisition parameters of the FASTMIT and CROP seismic surveys are reported in Table 1.

The very high-resolution CHIRP seismic profiles were acquired along the multibeam tracks with a hull-mounted sub-bottom profiler with sweeps ranging from 2 to 7 kHz and a vertical decimetric resolution. The morpho-bathymetric data were acquired with a hull-mounted multibeam sonar operating at a frequency of 100 kHz and illuminating a swath on the seafloor of 150° across track and 1.5° along track. To ensure data coverage, each swath overlapped the adjacent ones by about 25%. Furthermore, navigation was ensured by three integrated D-GPS systems. Six exploration boreholes (Oscar 1, Carla 1, Olga 1, Orione est 1, Venere 1 and Zagara 1, Fig. 2), available in the framework of the "Visibility of Petroleum Exploration Data in Italy" Project (ViDEPI, https://www.videpi.com/videpi/videpi.asp), were used to calibrate the MCS profiles.

4. Methods

To study the gas occurrence in the area, a series of analyses have been performed on different types of geophysical data. In particular, the MCS data have been processed with the flow described in Fig. 4, allowing the determination of detailed velocity fields and the imaging in time and depth of the gas-related anomalies. AVA analysis has been performed on specific horizons to identify the top of gas-bearing successions. CHIRP and bathymetric data have been processed in order to identify the gas presence in the shallower sediments and at the seafloor.

4.1. Multichannel seismic data processing

The processing flow of the MCS data (Fig. 4) was applied on the FASTMIT 6 line and on a part of the CROP M-23 A line. The procedure can be summarized as following: i) geometry assignment and zero-time correction; ii) band-pass filtering, both in time and Radon domain (Yilmaz, 2001), in order to increase the signal-to-noise ratio; iii) geometrical spreading correction; iv) manual removal of dead and noisy traces; v) predictive deconvolution, applied in order to reduce coherent noise such as seabed multiples; vi) semblance velocity analysis on gained (AGC, i.e. automatic gain control) common-mid-point (CMP) gathers; vii) pre-stack time Kirchhoff migration; viii) residual analysis on CMP gathers and update of the velocity field on the pre-stack migrated data; ix) normal move-out (NMO) correction and common-depth-point (CDP) stacking; x) computation of the classical

Table 1
Acquisition parameters for the FASTMIT and CROP seismic surveys.

Source			Streamer		
	FASTMIT	CROP		FASTMIT	CROP
Model	2 GI-guns	4 × × 8 AIR-guns	**Model**	Sercel Seal	Sercel SN-358-DMX
Array	11.6 l	80.4 l	**Length**	1.5 km	4.5 km
Shot interval	25 m	50 m	**N. of channels**	120/180	180
Depth	5 m	8 m	**Ch. distance**	12.5 m	25 m
			Depth	4 m	12 m
			Near offset	60 m	150 m
			Sampling rate	1 ms	4 ms

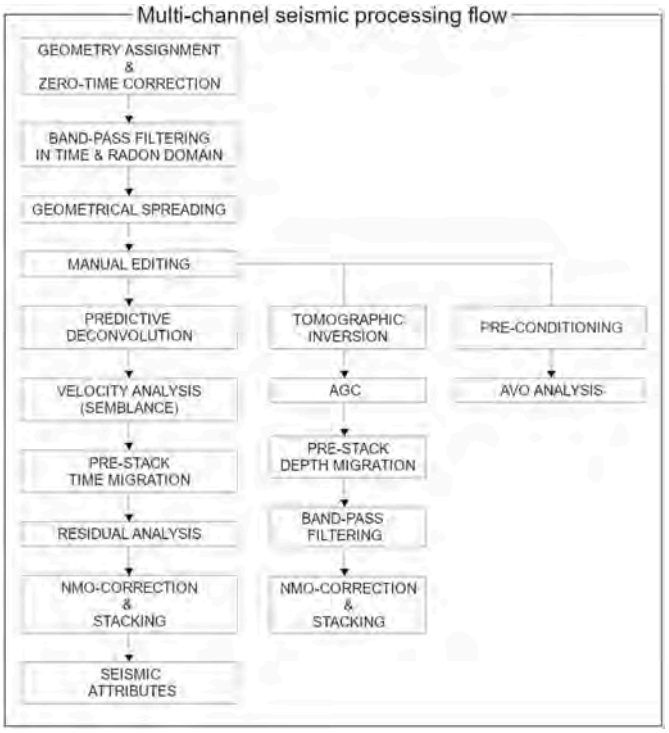

Fig. 4. Processing flow applied to the multi-channel seismic data.

instantaneous amplitude and instantaneous frequency attributes sections (Taner et al., 1979). Since the seismic acquisition was carried out at shallow water depths, the waveform frequency distortion caused by the NMO could severely damage the shallow events. Therefore, a close attention was paid to the stretch and mute application, obtaining adequate imaging and resolution also of the shallower structures. Furthermore, analysis of the near trace profiles (Fig. 5) highlighted coherent phase inversions at depth that can be related to a velocity decrease due to the presence of gas.

In addition to these processing steps, a tomographic approach was applied to provide an accurate estimation of the velocity fields, analysing the reflected arrivals along the main reflectors. The results of the tomographic inversion were used, after a further band-pass filtering, to perform a Kirchhoff pre-stack depth migration on AGC-gained CMP gathers. Moreover, as a further piece of evidence of the gas presence, an AVA analysis has been carried out on pre-conditioned CMP gathers.

To complement the study, a part of the MCS FASTMIT 3 line was processed in time domain and migrated with the pre-stack time Kirchhoff method, in order to be analyzed with the collocated CHIRP data (Ch73, Ch63, Ch50).

The whole processing was performed using the open-source Seismic Unix® software and the commercial Echos, Geodepth and Probe (Paradigm®) software.

4.1.1. *Seismic tomographic inversion and depth migration*

The tomographic inversion used in this work (applied on the FASTMIT 6 and on a part of the CROPM-23 A) is described in detail by Vesnaver et al. (1999). This procedure uses a modified version of the minimum time ray tracing developed by Böhm et al. (1999) and an iterative procedure for the inversion based on the Simultaneous Iterative Reconstruction Technique (SIRT) algorithm and on the staggered grids methods (Vesnaver and Bohm, 2000). The latter enhances the resolution of the inversion with respect to the acquisition geometry without increasing the null space energy of the tomographic system. The inversion was performed using a model with velocity pixels 0.5 km wide and interface sampling of about 0.5 km. Five and four main reflectors, characterized by high amplitude and considerable lateral continuity, were identified and inverted for the seismic lines FASTMIT 6 and CROP M-23 A, respectively. Various Common Image Gathers (CIGs) have been analyzed along the seismic profiles for a further checking and tuning of the tomographic velocity model. CIGs can be considered similar to move-out corrected CMP gathers (Accaino et al., 2005) and were used to make a residual correction in the velocity estimate at the analyzed location. The model updating is based on the CIG analysis and it is repeated until residual move-outs are reduced to a minimum. Finally, the Kirchhoff pre-stack depth migration of the two MCS lines was performed.

4.1.2. *Amplitude variation with angle*

The seismic attributes panels and the tomographic inversion evidenced the presence of gas-related features in both MCS profiles (see paragraphs 5.1 and 5.2). However, velocities and acoustic impedance variations do not provide sufficient evidence to confirm the presence of gas-filled reservoirs (Li et al., 2007). Instead, AVA/AVO techniques exploit relative changes in seismic amplitudes at varying incident angles/offsets to quantify changes in elastic properties. Elastic parameters are related to the fluid content and, therefore, AVA/AVO analysis can be applied in revealing gas-bearing formations/intervals. The technique is based on the Aki-Richards equation (Aki and Richards, 1980), which is a linear approximation of the Zoeppritz equations (Zoeppritz, 1919) for the reflection coefficient at the reflection interface. Shuey (1985) developed a simplified equation for the P-wave reflection as a function of the incident angle.

In this work, 2-parameters AVA inversion on NMO-corrected CMP gathers was performed in order to further constrain the gas distribution

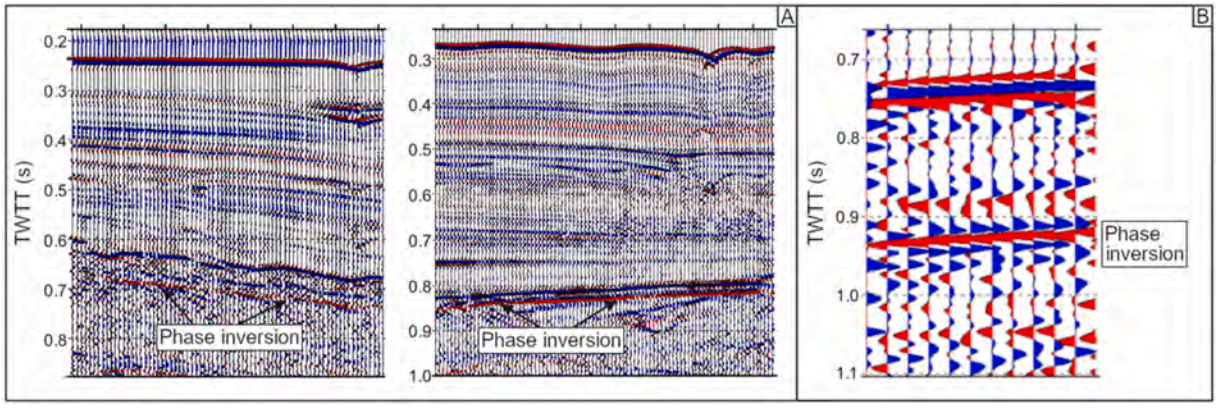

Fig. 5. Zoom of near-trace sections along A) the FASTMIT 6 and B) the CROP M-23 A multi-channel seismic lines. Coherent phase inversions are highlighted along horizons at 0.6–1 s of depth.

and to identify the top of gas-saturated zones and their depth. Input CMP gathers were pre-conditioned for the analysis but, in order to preserve the relative amplitudes of the reflected events, no gain filters, no deconvolution nor migration were applied. CMP were corrected for the NMO using the velocity fields from the tomographic inversion and, in order to avoid signal distortion deriving from the stretching effect, traces were muted beyond 50° of the modelled incidence angle. The mute beyond 50° can be considered sufficient as the shallowest investigated reflection was at about 600 ms and no stretch is present at angles smaller than 50°. Furthermore, a statistical procedure was applied in order to equalize amplitudes and wavelets across all offsets, under the basic assumption that the possible variations are the same for the entire seismic line (Jenner, 2002; Canning and Malkin, 2008). The equalizations were done in two steps: the training phase, in which the dataset was analyzed per offset and the operator for this offset was constructed; the application phase, in which the operator was applied to the data. The training was performed on a portion of the data of high quality (not affected by artifacts due to the absence of migration) and where no gas was expected. The objective of amplitude equalization was to find a single balancing scale factor for each offset. Data within the training zone were sorted to common offset gathers and the envelope was calculated for all traces. The amplitude operator was then calculated as the inverse of the RMS value of all envelope traces within each offset gather. The operator, different for each offset but single for all traces in that offset, was then applied. In the case of wavelet equalization, the data were first sorted into common offset gathers and then stacked into a single offset gather. A linear filter was then constructed for each input trace (offset) to map this trace to the trace at a reference offset. This was set as a medium offset, in such a way to be suitable for both small and medium angles and thus being able to determine both VP and VS.

Amplitudes of the pre-conditioned CMP gathers were then measured in a time window of 10 ms around 4 reflectors of interest and plotted as a function of angle of incidence. A global normalization was applied to each curve.

4.2. Bathymetric and CHIRP data processing

Bathymetric data, acquired with the Reson 8111 (frequency of operation of 100 kHz) and the Reson 7150 (frequency of operation of 12 kHz) multibeam echosounder systems, logged through the PDS 2000® acquisition software, was fully corrected for the ship's motion, navigation, sound velocity and tides. Onboard, sound velocity profiles were collected with a Sound Velocity Probe MiniSVP Valeport to correct for variations in the water column. The resulting Digital Terrain Model (grid cell size of 5 × 5 m) was edited (removal of residual spikes) and filtered. Data visualization was done using the GlobalMapper® software and the freely available GMT® (Generic Mapping Tools; Wessel and Smith, 1991).

CHIRP data was acquired with a Teledyne Benthos system and processed with the Echos Paradigm® software and Seismic Unix®. The altitude differences due to the sea waves were removed by applying a non-surface consistent static correction through a cross-correlation of each input trace with a pilot trace within a predetermined time window centered at the seafloor. After the static correction, the Hilbert transform was calculated to obtain the instantaneous amplitude section. The final CHIRP profiles yield a detailed image of the subsurface up to ~ 100 m of depth, depending on seafloor lithology and dip.

4.3. Seismo-stratigraphic interpretation

The seismo-stratigraphic interpretation of the MCS lines was performed through the recognition of key horizons associated with lithological changes and/or unconformities and bounding seismic units characterized by distinctive seismic features (e.g., amplitude, lateral continuity and frequency of internal reflectors). Such horizons were correlated with the stratigraphy derived from the hydrocarbon wells and literature information. The following reflectors, all characterized by a high value of acoustic impedance contrast, were clearly identified: the top of the Lower Pliocene Trubi Fm.; the Messinian Unconformity (or top of the Miocene); the top of the Meso-Cenozoic carbonate succession (only visible along the CROP M-23 A line). In particular, the Messinian Unconformity is seismically expressed by a rugged, high-amplitude and continuous reflector that is generally associated with a subaerial exposure (Messinian Erosional Surface, MES). The Trubi Fm. generally shows a semi-transparent seismic facies that makes this deposit well recognizable with respect to the less tectonized Upper Pliocene-Pleistocene siliciclastic succession formed by well-layered horizontal reflectors with low-to-high amplitude and high frequency. Furthermore, a high-amplitude discontinuous reflector is reported along the CROP M-23 A line, which has been interpreted as a magmatic sill intrusion by Civile et al. (2018). Lastly, the unconformity associated with the Last Glacial Maximum (LGM, *ca.* 20 ka B.P.) (Siddall et al., 2003; Clarke et al., 2009) has been recognized in all the CHIRP profiles.

5. Results

The results obtained from the seismic processing flow outlined in Fig. 4, together with the CHIRP and bathymetric data, are shown below. They are presented separately in the next paragraphs and jointly discussed afterwards.

5.1. Attributes sections

The instantaneous amplitude section obtained for the FASTMIT 6 line (Fig. 6A) highlights the presence of several anomalous zones in the Lower Pliocene succession. In particular, low amplitude zones are located below or in the vicinity of a seafloor characterized by the presence of negative morphologies (white dots in Fig. 6A and B), which can be interpreted as pockmarks, i.e. morphological depressions produced by the release of over-pressured fluids from the subsurface (Hovland et al., 2010).

In the SE part of the line, the presence of several aligned pockmarks, clearly visible also in the multibeam data (Fig. 2), can be associated with narrow vertical disturbances disrupting the Upper Pliocene-Pleistocene sediments. These are evident both in the instantaneous amplitude and in the instantaneous frequency sections (Fig. 6A and B). Moreover, an enhanced reflection (bright spot) is visible in the Upper Pliocene-Pleistocene deposits, below the pockmark positioned in the NW part of the line. This bright spot appears linked to a loss of high frequencies just below it (Fig. 6B). Another bright positive anomaly is present in the central part of the line, about 0.1 s above a transpressional structural high, mimicking the Messinian Unconformity shape (marked as 1 in Fig. 6A and B). High frequencies appear absorbed below it (Fig. 6B). Moreover, a 1.5 km-long high amplitude reflector is located in the Lower Pliocene succession (marked as 2 in Fig. 6A and B) south-eastward from the structural high marked as 1 in Fig. 6A and B. It also shows a loss of high frequency just below it. On the basis of well information (Venere 1 and Zagara 1 wells), this reflector could be produced by the velocity contrast at the interface between a mostly carbonate lower part and a marly/clayey upper part of the Trubi Fm.

The CROP M-23 A line shown in Fig. 6C and D crosses the area located between the CGFS to the west and the SFS to the east. In the central part of this line, the instantaneous amplitude and instantaneous frequency sections show several vertical anomalies in the Plio-Pleistocene succession (Fig. 6C and D). These features appear linked to the fractures affecting a thick high-amplitude reflector that was interpreted by Civile et al. (2018) as a possible seismic expression of an intrusive sheet of igneous material (i.e., a sill intrusion). In the Miocene succession, at a depth of about 1 s, a high-amplitude reflector is visible below the potential sill intrusion. This is also recognizable in the near-trace section, where it shows reversed polarity (Fig. 5B), suggesting gas accumulation. High frequencies are absorbed below this reflector. In

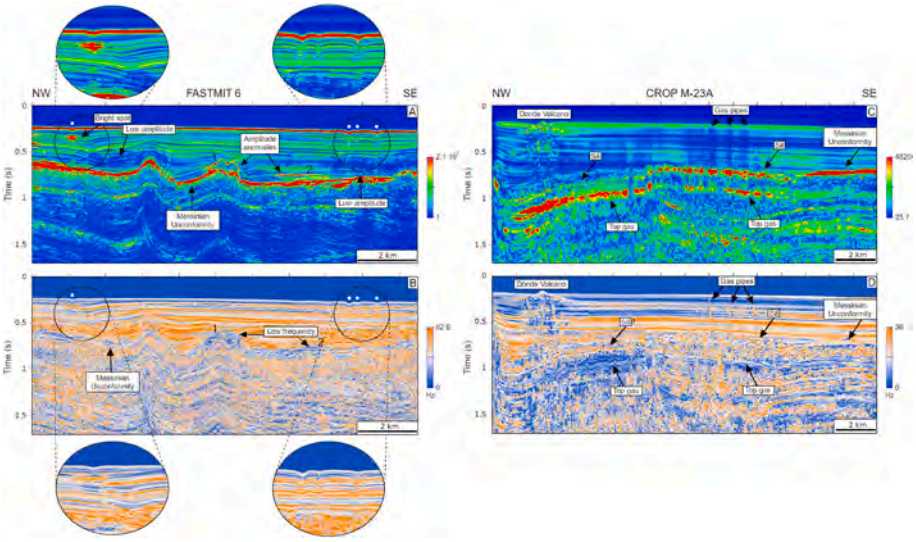

Fig. 6. A) Instantaneous amplitude and B) instantaneous frequency seismic attributes for the FASTMIT 6 seismic line. White dots indicate pockmarks; the black box highlights the presence of vertical disturbances that can be related with the presence of gas. Amplitude and frequency anomalies are indicated by arrows and horizons 1 and 2 are indicated (see text for details). The Messinian Unconformity is marked. C) Instantaneous amplitude and D) instantaneous frequency seismic attributes for the CROP M-23 A seismic line. Gas pipes are highlighted. The Doride Volcano, the magmatic sill intrusion and the Messinian Unconformity are marked. The top of the possible gas-bearing formation is indicated (Top gas).

the NW part of the line, at ~1 s depth, high frequencies are also lacking (Fig. 6D).

5.2. Depth migrated sections and tomographic results

5.2.1. FASTMIT 6 multi-channel seismic line

Fig. 7A shows the pre-stack depth migration of the FASTMIT 6 line superimposed on the obtained tomographic velocity field, whereas the seismo-stratigraphic and structural interpretation of the same seismic section is reported in Fig. 8, along with the recognized gas-related features. Fig. 8 shows the presence of three different seismic facies which, from bottom to top, are associated with the Miocene, Lower Pliocene and Upper Pliocene-Pleistocene respectively. A tectonic deformation produced by the development of positive flower structures mainly deforms the pre-Upper Pliocene succession. These transpressional zones

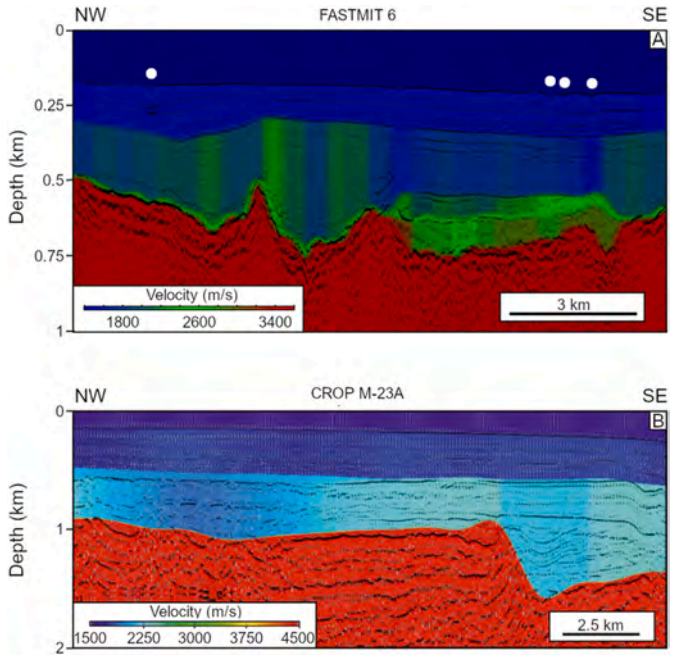

Fig. 7. Pre-stack depth migration section superimposed on the calculated tomographic velocity field for A) the FASTMIT 6 and B) a part of the CROP M-23 A seismic lines (see text for details). White dots indicate the presence of pockmarks. Low-velocity zones are recognizable in both lines.

can be related with the tectonic activity of the CGFZ. The tomographic inversion of the main reflected events (Fig. 7A) shows velocity values ranging between 1550 and 1600 m/s in the shallowest sediments along the entire seismic profile. The Lower Pliocene succession is characterized by fairly consistent lateral velocity variations, with an extensive low velocity area (about 1600–1650 m/s) in the SE sector. In the central and NW sectors, vertically extended low-velocity zones are visible (Fig. 7A). Buried negative morphologies are visible at a depth ranging between 0.3 and 0.4 km in the NW part of the seismic line (Fig. 8). These features can be interpreted as "advancing" paleo-pockmarks, e.g. paleo-pockmarks with laterally migrating infill geometries (Ho et al., 2018; Kumar et al., 2021), and indicate past fluid escape. Interestingly, these paleo-pockmarks appear related to a Pliocene fault which may have acted as a preferential path for the rising gas. Furthermore, they are located at about 0.5 km toward SE with respect to the north-westermost pockmark identified in the attributes sections (Fig. 6A and B), below which there is a bright spot, suggesting local gas accumulation (Fig. 6A and B, Fig. 8). All the other pockmarks and the narrow vertical pipes described in paragraph 5.1, distinguishable down to a depth of about 0.4 km (i.e., the top of the Lower Pliocene succession), are clearly visible and can be related with the gas migration (Fig. 8). The top of the Lower Pliocene, located at a depth of about 0.4 km, marks a significant change in the seismic facies mostly in the areas affected by transpressional deformations.

5.2.2. CROP M-23 A multi-channel seismic line

Fig. 9 shows the pre-stack depth migration of the part of the CROP M-23 A line crossing the area between the CGFZ and SFZ. The Doride volcanic edifice (Lodolo et al., 2019) is located at the NW border of the line along with the associated buried volcanic deposits. The Plio-Pleistocene succession, in the north-westernmost part of the line, is characterized by multiple sub-vertical blanking, likely related to rising fluids phenomena. The south-easternmost part of the line shows the faults associated with the SFS that constitute the western boundary of the Gela foredeep basin. The already mentioned sill intrusion is found at a depth between 0.6 and 0.9 km in the NW and central parts of the line. Given its depth and thickness, this horizon is able to mask the top of the Miocene (Messinian Unconformity), which cannot be resolved. The sill intrusion is highly fractured and is interrupted by a 0.5 km-wide vertical zone characterized by a chaotic signal, possibly associated with a magmatic ascent. The tectonized top of the Meso-Cenozoic carbonate succession is identifiable at depths between 1 and 1.5 km (Fig. 9), correlating with the absence of the sill.

The tomographic inversion of the main reflections up to the top of

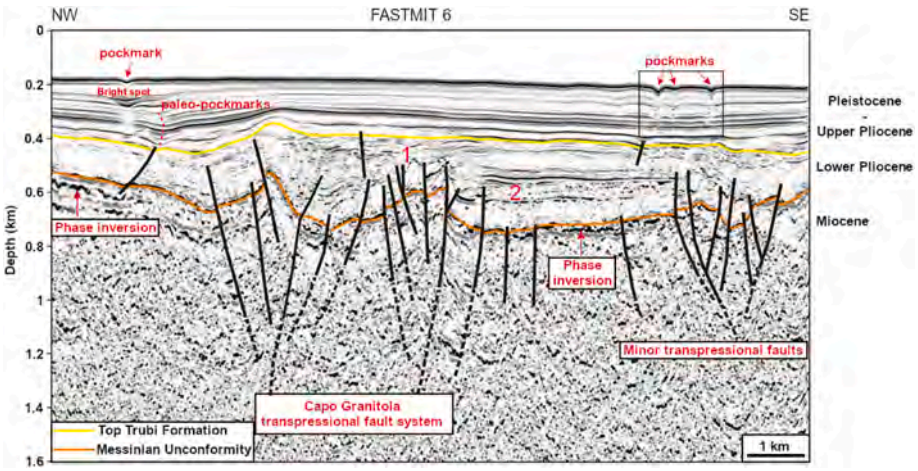

Fig. 8. Seismo-stratigraphic and structural interpretation of the FASTMIT 6 seismic line, with the main recognized gas-related features. The black box highlights the presence of gas pipes, the horizons 1 and 2 are marked, the phase inversion related to the top of the gas-bearing formation is indicated (see text for details).

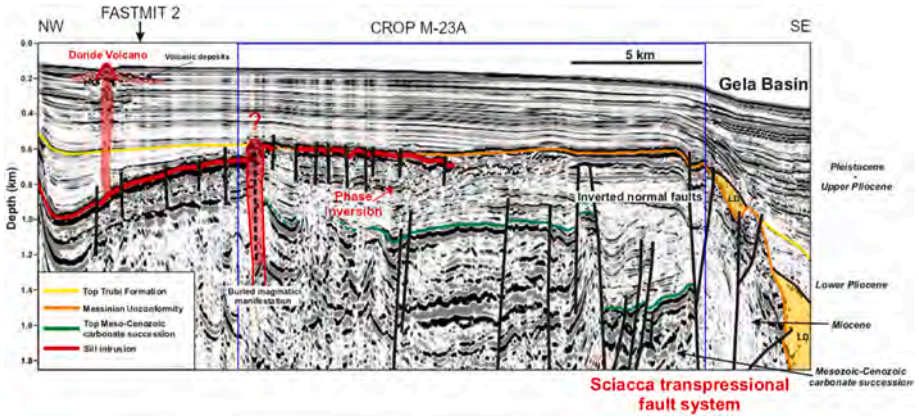

Fig. 9. Seismo-stratigraphic and structural interpretation of the CROP M-23 A seismic line (bold green line in Fig. 2), with the main recognized gas-related features. The blue box highlights the part of the line where the tomographic inversion has been performed (see Fig. 7B). The phase inversion related to the top of the possible gas-bearing formation is indicated (see text for details). Abbreviation: LD, landslide deposit. (For interpretation of the references to colour in this figure legend, the reader is referred to the Web version of this article.)

the Meso-Cenozoic carbonate succession was performed in the central part of the seismic line (Fig. 7B). The most significant result is the velocity inversion between the reflection at about 0.7 km and the top of the Meso-Cenozoic carbonate succession. Furthermore, analyzing the wavelets between these two main reflectors, a phase inversion at depth of about 0.9 km is evident. This phase inversion is also clearly visible in the near trace shown in Fig. 5B. In the SE part of the seismic line, there is another velocity decrease in the sediments above the carbonate succession located close to the edge of the Gela Basin (Fig. 7B).

5.3. Amplitude variation with angle

The variation in amplitude of a seismic reflection with incident angle (AVA) was analyzed for 2 reflectors, one for each MCS line, associated with a phase inversion and characterized by significant amplitude information. Furthermore, the AVA behaviour was plotted for the Messinian Unconformity and the Lower Pliocene horizon belonging to the Trubi Fm. of the FASTMIT 6 line (Horizon 2), to provide a reference for formations where no gas is expected. Fig. 10 shows the AVA curves before and after the CMP gather pre-conditioning described in the paragraph 4.1.2, together with the theoretical response in the Shuey (1985) approximation. Fig. 10A and B shows the AVA response obtained along the FASTMIT 6 line for the Messinian Unconformity and for the Lower Pliocene horizon identified by the attributes analysis (Horizon 2 in Fig. 6A and B). In both cases, amplitude decreases with incident angle and it changes in polarity at around 30°–35° of the incident angle (Fig. 10A and B).

Fig. 10C and D shows the AVA responses for the reflector characterized by a phase inversion identified just below the Messinian Unconformity both in the FASTMIT 6 (Fig. 10C) and in the CROP M-23 A (Fig. 10D) lines. In both cases, polarity is negative and amplitude decreases in absolute value with the incident angle, eventually changing in sign (for angles >30° in the case of the FASTMIT 6 line and for angles >50° in the case of the CROP M-23 A line). This behaviour can be ascribed to the gas presence and it has been classified, following Castagna et al. (1998), as an AVO class 4 anomaly. A class 4 anomaly normally involves low impedance, uncompacted and unconsolidated gas sands overlain by high impedance cap rocks like hard, siliceous or calcareous shales, siltstones or tightly cemented sands or carbonates. In the analyzed seismic profiles, both the sill intrusion and the Messinian Unconformity can be considered good cap rocks candidates.

5.4. Bathymetric and very high-resolution seismic data

The integrated analysis of the multibeam and CHIRP data allowed the identification on the seafloor and in the shallow subsurface of peculiar morphologies linked to gas migration.

An extensive pockmark field (~40 depressions) develops for 25 km in a NW-SE direction from the Nerita Bank to the NW part of the FASTMIT 6 line and then bends southwards (Fig. 2). The pockmarks have a V-shaped profile and are sub-circular at the seafloor, although few slightly elliptical depressions have been identified. The CHIRP profiles (Ch216-220 in Fig. 2) acquired along the FASTMIT 6 line and the overlapping multibeam data show the presence of more depressions on the seafloor

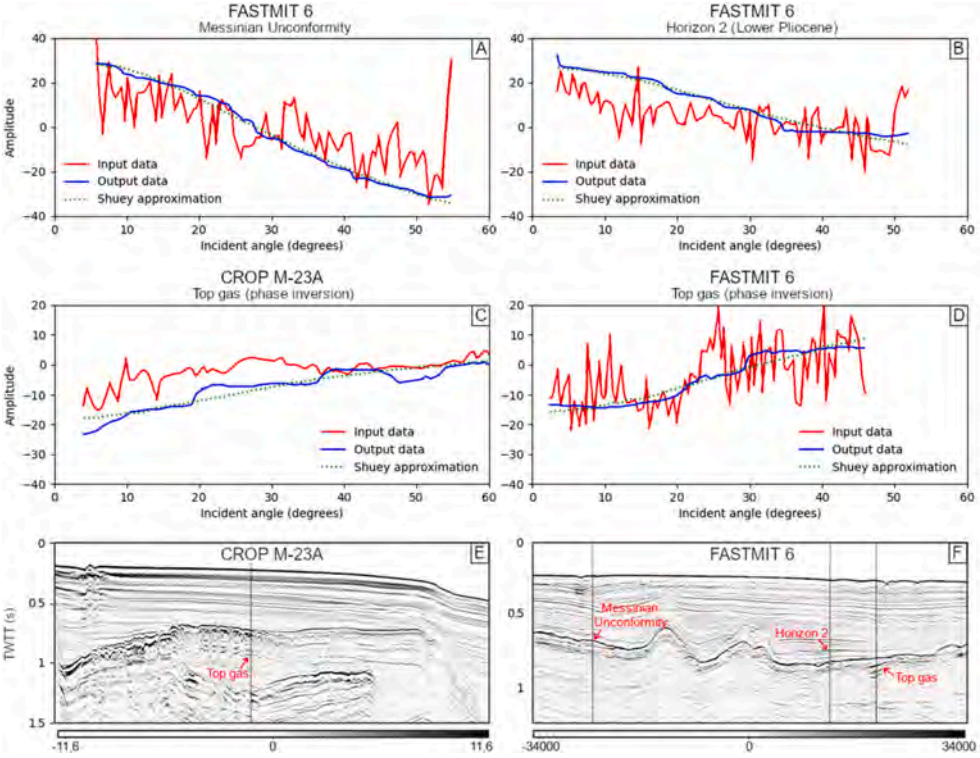

Fig. 10. AVA plots for A) the Messinian Unconformity along the FASTMIT 6 line; B) the top of the possible gas-bearing formation along the CROP M-23 A line where the phase inversion has been recognized; C) the Lower-Pliocene Horizon 2 along the FASTMIT 6 line; D) the top of the possible gas-bearing formation along the FASTMIT 6 line where the phase inversion has been recognized; E) and F) the CROP M-23 A and the FASTMIT 6 seismic line in TWTT (not migrated) with the analyzed horizons marked.

than the ones recognized in the MCS profile (marked from 1 to 8 in Fig. 11). The north-westernmost pockmark (1 in Fig. 11) is localized above a gas pipe characterized by an inflection of the seismic reflectors in the CHIRP data (Fig. 11), corresponding to a velocity pull-down effect, and by acoustic turbidity. The wavy stratification visible in the SE sector of the CHIRP data is produced by the presence of the pockmarks (marked from 3 to 7 in Fig. 11). Gas pipes are evident for two of these features (5 and 7 in Fig. 11) and shallow local high-amplitude reflections beneath the seafloor indicate the presence of a temporary gas accumulation.

The analysis of the multibeam and CHIRP data also highlights the presence of positive features located in the NE sector of the study area (Figs. 12 and 13). In particular, the data reveal partially buried low reliefs forming a 2 km-long, NS-oriented alignment, which are locally visible at the seafloor where they form three clusters (Figs. 13 and 12). The water depth of their summit is around 60 m, whereas their height on the seafloor ranges between 1 and 7 m (Fig. 12). The major mound covers an area of 0.032 km^2 (Fig. 12). The three CHIRP profiles reported in Fig. 13 (Ch73, Ch63, Ch50) cross the alignment from north to south showing the characteristics of these mounds. They are characterized by a rugged top morphology and present an opaque seismic facies that does not allow a good signal penetration. Moreover, they lie on a folded pre-LGM succession, and in particular along the hinge of an anticline. The CHIRP line Ch73 (Fig. 13A) shows the north-east mound, which appears active and deforms the present-day sedimentary cover and the seafloor. The buried morphological profile of the mound is different with respect to the outcropping part, possibly because of the presence of gas emissions recognizable at the top of the structure and in the water column (gas flares). The CHIRP line Ch63 (Fig. 13B) shows a pronounced buried mound that deforms the surrounding sediments. The CHIRP line Ch50 (Fig. 13C) shows a buried mound and several bright spots above the LGM unconformity associated with zones of signal blanking, interpreted as gas-related features. The presence of gas is confirmed by flares in the water column.

A further isolated mound, the major of the study area, is located 800 m eastward from the Actea Volcano (Lodolo et al., 2019) (Fig. 2) at water depths between 77 and 81 m. It covers an area of 0.155 km^2 and presents a maximum height of 10 m. This mound shows the same morphological and acoustic features of the above-mentioned reliefs and a significant gas seeping is visible along its SW side (CHIRP line Ch100 in Fig. 14). The sedimentary succession covering the flanks of the mound appears deformed suggesting, also in this case, a very recent activity.

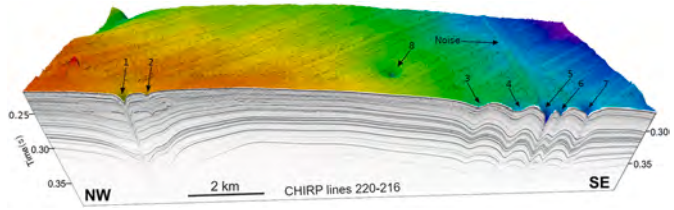

Fig. 11. A combined set of CHIRP profiles (220–216) located along the FASTMIT 6 seismic line is displayed along with the bathymetry (see Fig. 2 for location). The recognized pockmarks are indicated with numbers from 1 to 8.

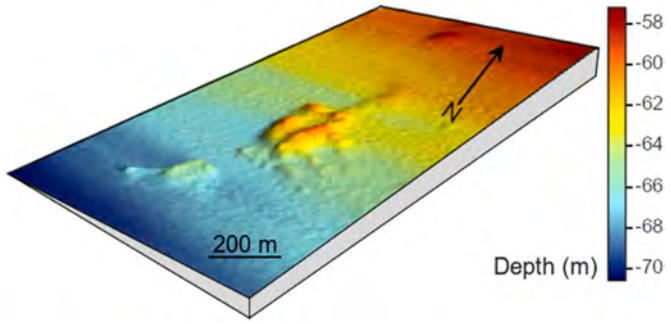

Fig. 12. Bathymetric data showing the mounds outcropping in the NE sector of the study area and arranged in three main clusters (see Fig. 2 for location) aligned along a N–S direction.

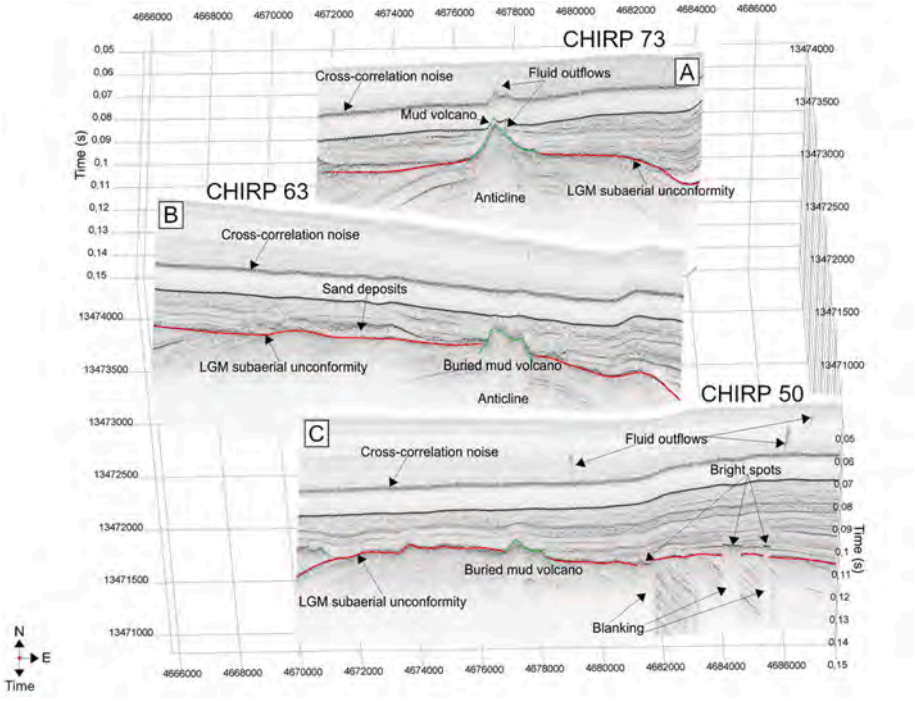

Fig. 13. Composite figure showing three E-W oriented CHIRP profiles (CHIRP 73, 63, 50) crossing the area characterized by the presence of outcropping and buried mounds located in the NE sector of the study area. These low reliefs lie along the hinge of an anticline and form a 2 km-long, NS-oriented, alignment. The gas-related features are highlighted, the LGM subaerial unconformity is marked. See Fig. 2 for location.

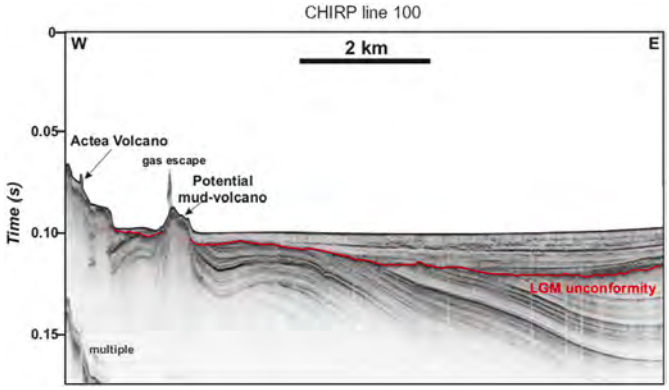

Fig. 14. The CHIRP line 100 showing the presence of a potential mud-volcano in the vicinity of the Actea Volcano. A gas flare is clearly recognizable in the water column. See Fig. 2 for location.

6. Discussion

The integrated interpretation of bathymetric, very high-resolution seismic and MCS data, have allowed the identification of gas-related features in the entire Miocene-Quaternary sedimentary succession and at the seafloor in the Capo Granitola-Sciacca offshore sector of the NW Sicilian Channel.

6.1. Seafloor and sub-seafloor gas expressions

Buried and outcropping mounds have been recognized in NW and NE sectors of the study area along the northern part of the CGFZ and SFS (Figs. 2, 12 and 13). These structures are not associated with magnetic anomalies and they are characterized by an opaque seismic facies without any visible internal reflectors. Moreover, they are associated with gas emissions in the water column, gas-related features in the subsurface (bright spots, zones of signal blanking) and deform both the recent sediments surrounding them and the seafloor, testifying for an active fluid flow system. In particular, the mounds located in the NE sector of the study area form a field characterized by several highs developed along a 2 km long, N–S alignment that lies on the hinge of an anticline related to the tectonic deformation produced by the faults of the SFS (Figs. 12 and 13). These reliefs can be interpreted as mud volcanoes generated by the rising of overpressure fluids and mud material along the faults and fractures associated with the active CGFS and SFS. Fig. 15 shows part of the time-migrated FASTMIT 3 line crossing the

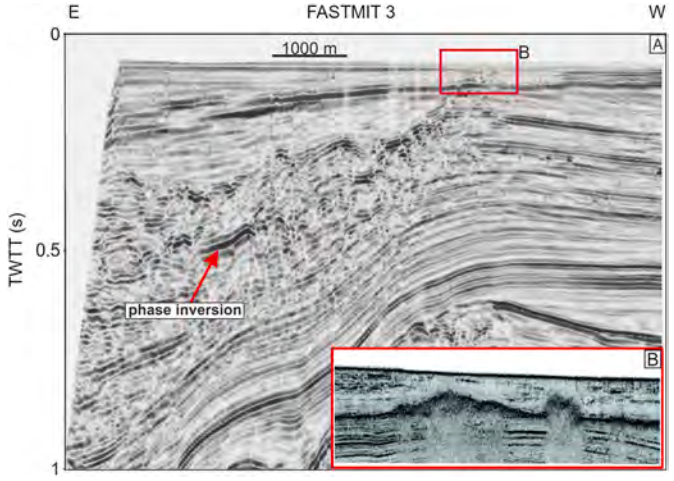

Fig. 15. A) Part of the FASTMIT 3 seismic line (bold blue line in Fig. 2) after pre-stack time migration. The line crosses the northern part of the mud volcanoes field located along the SFS. A phase inversion is highlighted on the east of the structure, at 0.5 s of depth. The red box shows the location of the CHIRP profile reported in B). B) The CHIRP profile clearly shows two buried mud volcanoes which are not easily interpretable in A). (For interpretation of the references to colour in this figure legend, the reader is referred to the Web version of this article.)

northern part of the mud volcanoes field located along the SFS (Fig. 2). A phase inversion on the east of the structure, at 0.5 s, suggests a deep origin for the involved gas, which could locally reach impermeable layers where it accumulates (Fig. 15).

Another gas expression visible on the seafloor and in the CHIRP data is represented by pockmarks. The bathymetric data allowed the identification of 42 pockmarks in the southern part of the study area between the Nerita Bank and the CGFZ.

They form a 25 km-long, NW-SE alignment, except for the westernmost sector, where their distribution bends southwards (Fig. 2). A probable tectonic control operated by a buried WNW-trending normal fault and by the transpressional structures associated with the CGFS might explain these two trends (see Civile et al., 2018). Although not showing any evidence of active emission in the water column, these pockmarks are not draped by recent sediments. This may have different explanations: they may be dormant or calm-flux seeps pockmarks (Dimitrov and Woodside, 2003), or they may be characterized by a cyclical behaviour of the gas emissions. In the last case, their origin could be traced in the hydrothermal activity related to the magmatism, which has been documented by both ROV observation and high-frequency seismic events recorded from July 2012 to March 2013 in the Graham Bank (Coltelli et al., 2016). In addition, the concurrence of bottom current processes could play a role in preventing the sediment deposition in the seafloor depressions.

The FASTMIT 6 line and the CHIRP data (Figs. 8 and 11) show that pockmarks are generally associated with the occurrence of vertical gas pipes and, in some cases, with local gas accumulations below the seabed, evidenced by bright spots (Figs. 6A and 8). In the first case (pockmark 1 in Fig. 11), it has been possible to reconstruct the seepage history through the recognition of "advancing" paleo-pockmarks in the Upper Pliocene-Pleistocene succession, which were most likely fed by gas that exploited a Pliocene fault rooted in the Miocene (Fig. 8). These features suggest that gas was temporarily accumulated below the paleo-seafloor several times in the past, causing its collapse. Indeed, hydrocarbon exploration data offshore south Sicily suggest that multiple periods of hydrocarbon migration and trapping have occurred in this area (Granath and Casero, 2004). The lateral migration of the paleo-pockmarks should reflect the interplay between intensity of paleo fluid leakage, pre-existing seabed topography and bottom currents. This is also the case of the advancing pockmarks composed of multiphase, migrated infill-sets observed above gas-bearing channels and deep-seated extensional faults in the Lower Congo Basin (Ho et al., 2018).

6.2. Deep gas

Along the FASTMIT 6 and the CROP M23A seismic lines, several 0.5–0.8 km-deep phase inversions (Figs. 5, 8 and 9) have been recognized and associated with an Upper Miocene horizon characterized by a high acoustic impedance contrast. It presents a class 4 AVO response with negative intercept and positive gradient in the Shuey (1985) approximation, likely indicating the top of a gas-bearing deposit. This reflector is not continuous enough to be inverted in the tomographic analysis but it develops over large parts of both the MCS near-trace sections (Fig. 5). In the SE part of the CROP M-23–A, a velocity decrease occurs in the sediments above the carbonate succession located close to the edge of the Gela Basin (Fig. 9). This anomaly is probably linked to the rise of fluid along the faults of the SFS. The top of the gas-bearing deposits (i.e., the reservoirs) is located just below a high-amplitude reflector interpreted as a strongly fractured sill intrusion. The gas leaks from gas-bearing layers located in the Miocene succession through the fractures and rises in the Plio-Pleistocene succession, causing strong vertical signal blanking up to the seafloor. In the FASTMIT 6 line (Fig. 8), the top of gas is recognizable below the Messinian Unconformity, where the fluid is able to accumulate. Locally, it is able to bypass the Messinian Unconformity through the sub-vertical faults associated with the identified positive flower structures (Fig. 8). In fact, the presence of pipes can be related to the transpressional structures deforming the pre-Upper Pliocene succession. These focused pathways cross-cut the entire Plio-Pleistocene succession producing local accumulations, highlighted by the presence of bright spots and pockmarks. Furthermore, the FASTMIT 6 tomographic results (Fig. 6A) show a 5 km-wide gas-induced low-velocity zone in the Plio-Pleistocene in the vicinity of the pockmarks recognized in the SE part of the line. This suggests an additional diffuse presence of gas, which is able to reduce the velocity.

6.3. Origin of gas and possible play

The results presented in this work mainly suggest a thermogenic deep origin for the gas included in the analyzed Miocene-Pleistocene succession. However, considering the presence of a Late Pleistocene to Holocene submarine volcanism (Cavallaro and Coltelli, 2019; Lodolo et al., 2019, 2021), a potential mixing with fluids of magmatic origin cannot be excluded. The only chemical analyses available in the area are related to a gas sample collected from the seafloor in proximity of the Graham Bank by Coltelli et al. (2016). The chemical composition and the ratios among different elements and isotopes of the sample reflects a clear magmatic/crustal origin. The molecular composition and the isotope signature of the methane present in the sample are consistent with a derivation of hydrocarbon gases by thermal cracking of organic matter, probably related to thermo-metamorphic reaction of limestone occurring in the deep crust (Coltelli et al., 2016). In any case, considering the Late Quaternary-Holocene age of volcanism, it is believed that the source history of the deep and of any magmatism-related gases are independent. However, the available dataset does not allow to discriminate the potential various gases contributions. The deep gas recognized in this study might have originated from the shaly intercalations recognized in the Meso-Cenozoic carbonate succession, which hosts the main reservoirs recognized in the Sicilian Channel (Civile et al., 2013). Possible source rocks could belong to the Oligocene-Lower Miocene Bonifato Fm., which host clayey intercalation, as reported in the Orione Est1 well, or to the Upper Cretaceous-Eocene Amerillo Fm., which comprises marly intercalations, as reported in the Venere1 well (see well locations in Fig. 2). To the NW of the study area, in the Nilde e Narciso oil fields (Fig. 1), the source rock is considered to consist of Late Triassic black shales (Granath and Casero, 2004). The deep gas appears able to exploit the lithospheric faults of the CGFS and SFS feeding high porosity and permeability Miocene and Pliocene-Quaternary horizons, which might by be represented by thin sandy and carbonate intercalations included in the Terravecchia and Ribera formations. The Late Miocene Terravecchia Fm. has been recognized as a gas-producing reservoir in other plays in Sicily, as reported by Granath and Casero (2004). Furthermore, two boreholes drilled in the study area (Venere 1 and Zagara 1, see location in Fig. 2) report several methane manifestations in the Ribera Fm. The Quaternary tectonics and the volcanism associated with the CGFZ and SFS likely produced the opening of additional preferential paths for the migration in the shallow subsurface of the deep gas.

Finally, a further mixing with shallow microbial gases might have happened. Indeed, in the Sciacca-Agrigento offshore, SE of the area of study (Fig. 1), Mancuso and Catalano (2020) reports microbial gases in the Upper-Pleistocene-Holocene deposits, derived from fluvial organic material. Their formation is due to the progressive sinking of the continental platform, with the consequence of shifting the deltaic environments onshore.

7. Conclusions

This work investigated the occurrence of gas in the Miocene-Pleistocene succession off the coast of SW Sicily, in the NW Sicilian Channel. Data from 3 multi-channel seismic profiles, 9 very high-resolution sub-bottom profiles and multibeam bathymetry have been

processed and integrated. Moreover, 6 hydrocarbon exploration wells were used to constrain the seismic interpretation and characterize the lithology of the stratigraphic succession. Multi-channel seismic data were processed in order to identify the signature of gas accumulation and migration. Through the recognition of velocity and/or amplitude anomalies, techniques such as inversion tomography and amplitude-with-angle analysis have been used to provide further details on the gas presence. Gas-related features, such as bright spots, gas chimneys and dimmed amplitude zones, were identified in the whole Miocene-Pleistocene succession. The top of gas-bearing deposits is located in the Upper Miocene. The gas migrated in the Plio-Pleistocene succession through sub-vertical faults and fractures. The very high-resolution seismic and bathymetric data showed the morphological and paleo-morphological expressions of the gas seeping from the seabed (i.e. pockmarks and advancing pockmarks, mud-volcanoes).

Considering the presented results, the literature information and the origin of the hydrocarbon fields exploited in the Sicilian Channel, a thermogenic deep origin is mainly suggested for the gas identified in the Miocene-Pleistocene succession of the study area. It may have been generated by shaly and marly intercalations hosted in the Meso-Cenozoic carbonate succession, possibly belonging to the Bonifato and Amerillo formations. The upward gas migration occurred along the roughly N–S oriented lithospheric faults associated with the Capo Granitola Sciacca Fault Zone (CGSFZ), and this allowed local accumulation in Miocene-Quaternary sandy and carbonate layers of the Terravecchia and Ribera formations. The Quaternary tectonics and the volcanism associated with the CGSFZ likely produced the opening of additional preferential paths for the accumulation in the shallow subsurface of deep gas and its migration at the seafloor. In any case, a potential mixing with shallow microbial gas or magmatism-related fluids cannot be excluded.

Declaration of competing interest

The authors declare that they have no known competing financial interests or personal relationships that could have appeared to influence the work reported in this paper.

References

Accaino, F., Böhm, G., Tinivella, U., 2005. Tomographic inversion of common image gathers. First Break 23, 39–44.

Aki, K., Richards G., P., 1980. Quantitative seismology: Theory and methods. W.H. Freeman, San Francisco.

Antonelli, M., Franciosi, R., Pezzi, G., Querci, A., Ronco, G.P., Vezzani, F., 1988. Paleogeographic evolution and structural setting of the northern side of the Sicily Channel. Memorie Società Geologica Italiana 41, 141–157.

Argnani, A., 1990. The Strait of Sicily rift zone: foreland deformation related to the evolution of a back-arc basin. J. Geodyn. 12, 311–331.

Argnani, A., 2009. Evolution of the southern Tyrrhenian slab tear and active tectonics along the western edge of the Tyrrhenian subducted slab. In: Van Hinsbergen, D.J.J., Edwards, M.A., Govers, R. (Eds.), Collision and Collapse at the Africa–Arabia–Eurasia Subduction Zone, vol. 311. Geological Society, London, Special Publications, pp. 193–212.

Argnani, A., Cornini, S., Torelli, L., Zitellini, N., 1986. Neogene-quaternary foredeep system in the strait of sicily. Memorie Società Geologica Italiana 36, 123–130.

Boccaletti, M., Cello, G., Tortorici, L., 1987. Transtensional tectonics in the sicily channel. J. Struct. Geol. 9, 869–876.

Böhm, G., Rossi, G., Vesnaver, A., 1999. Minimum-time ray-tracing for 3-D irregular grids. J. Seismic Explor. 8, 117–131.

Calò, M., Parisi, L., 2014. Evidence of a lithospheric fault zone in the Sicily Channel continental rift (southern Italy) from instrumental seismicity data. Geophys. J. Int. 199 (1), 219–225.

Calò, M., Parisi, L., Luzio, D., 2013. Lithospheric P- and S-wave velocity models of the Sicilian area using WAM tomography: procedure and assessments. Geophys. J. Int. 195 (1), 625–649. https://doi.org/10.1093/gji/ggt252.

Canning, A., Malkin, A., 2008. Removing NMO/migration stretch effects for improved AVO analysis. In: Hyderabad-2008 - 7th Conference & Exposition on Petroleum Geophysics (India).

Carminati, E., Lustrino, M., Doglioni, C., 2012. Geodynamic evolution of the central and western Mediterranean: tectonics vs. igneous petrology constraints. Tectonophysics 579, 173–192. https://doi.org/10.1016/j.tecto.2012.01.026.

Cartwright, J., 2007. The impact of 3D seismic data on the understanding of compaction, fluid flow and diagenesis in sedimentary basins. J. Geol. Soc. 164, 881–893. https://doi.org/10.1144/0016-76492006-143.

Casero, P., 2004. Structural setting of petroleum exploration plays in Italy. In: Crescenti, V., D'Offizi, S., Merlino, S., Sacchi, L. (Eds.), Geology of Italy, Special Volume of the Italian Geological Society for the IGC 32 Florence-2004, pp. 189–199.

Castagna, J.P., Swan, H.W., Foster, D.J., 1998. Framework for AVO gradient and intercept interpretation. Geophysics 63, 948–956.

Catalano, R., Infuso, S., Sulli, A., 1993. The Pelagian Foreland and its northward Foredeep. Plio-Pleistocene structural evolution. In: Max, M.D., Colantoni, P. (Eds.), Geological Development of the Sicilian-Tunisian Platform. Proceedings of International Scientific Meeting, vol. 58. University of Urbino, Italy, pp. 37–42, 4–6 November, 1992. Unesco Report in Marine Science.

Cavallaro, D., Coltelli, M., 2019. The Graham volcanic field offshore southwestern sicily (Italy) revealed by high-resolution seafloor mapping and ROV images. Front. Earth Sci. 7 https://doi.org/10.3389/feart.2019.00311.

Civile, D., Lodolo, E., Accettella, D., Geletti, R., Ben-Avraham, Z., Deponte, M., Facchin, L., Ramella, R., Romeo, R., 2010. The Pantelleria graben (Sicily Channel, Central Mediterranean): an example of intraplate 'passive' rift. Tectonophysics 490, 173–183.

Civile, D., Lodolo, E., Accaino, F., Geletti, R., Schiattarella, M., Giustiniani, M., et al., 2018. Capo granitola-sciacca fault zone (Sicilian Channel, Central Mediterranean): structure vs magmatism. Mar. Petrol. Geol. 96, 627–644. https://doi.org/10.1016/j.marpetgeo.2018.05.016.

Cavallaro, D., Monaco, C., Polonia, A., Sulli, A., Di Stefano, A., 2017. Evidence of positive tectonic inversion in the north-central sector of the Sicily Channel (central Mediterranean). Nat. Hazards 86, S233–S251.

Civile, D., Brancolini, G., Lodolo, E., Forlin, E., Accaino, F., Zecchin, M., Brancatelli, G., 2021. Morphostructural setting and tectonic evolution of the central part of the Sicilian channel (central mediterranean). Lithosphere 2021 (1), 7866771. https://doi.org/10.2113/2021/7866771.

Civile, D., Lodolo, E., Alp, H., Ben-Avraham, Z., Cova, A., Baradello, L., Accettella, D., Burca, M., Centonze, J., 2014. Seismic stratigraphy and structural setting of the Adventure Plateau (Sicily Channel). Mar. Geophys. Res. 35 (1), 37–53. https://doi.org/10.1007/s11001-013-9205-5.

Civile, D., Zecchin, M., Forlin, E., Donda, F., Volpi, V., Merson, B., Persoglia, S., 2013. CO_2 geological storage in the Italian carbonate successions. Int. J. Greenh. Gas Contr. 19, 101–116. https://doi.org/10.1016/j.ijggc.2013.08.010.

Clarke, P.U., Dyke, A.S., Shakum, J.D., Carlson, A.E., Clark, J., Wohlfarth, B., Mitrovica, J.X., Hostetler, S.W., McCabe, A.M., 2009. The last glacial maximum. Science 325, 710–714.

Colantoni, P., Del Monte, M., Gallignani, P., Zarudzky, E.F.K., 1975. Il Banco Graham: un vulcano recente nel Canale di Sicilia. Giorn. Geol. 40 (1), 141–162.

Coltelli, M., Cavallaro, D., D'Anna, G., D'Alessandro, A., Grassa, F., Mangano, G., Patanè, D., Gresta, S., 2016. Exploring the submarine Graham Bank in the sicily channel. Ann. Geophys. 59 (2) https://doi.org/10.4401/ag-6929.

Corti, G., Cuffaro, M., Doglioni, C., Innocenti, F., Manetti, P., 2006. Coexisting geodynamic processes in the sicily channel. In: Dilek, Y., Pavlides, S. (Eds.), Postcollisional Tectonics and Magmatism in the Mediterranean Region and Asia, vol. 409. Geological Society of America, pp. 83–96 (Special Paper).

Davis, A.M., 1992. Shallow gas: an overview. In: Davis, A.M. (Ed.), Methane in marine sediments, Continental Shelf Research 12, 1077–1079.

Di Stefano, E., Infuso, S., Scarantino, S., 1993. Plio-Pleistocene sequence stratigraphy of south western offshore Sicily from well-logs and seismic sections in a high resolution calcareous plankton biostratigraphic framework. In: Max, M.D., Colantoni, P. (Eds.), Geological Development of the Sicilian-Tunisian Platform. Proceedings of International Scientific Meeting, vol. 58. University of Urbino, Italy, pp. 105–110, 4–6 November, 1992. Unesco Report in Marine Science.

Dimitrov, L., Woodside, J, 2003. Deep sea pockmark environments in the eastern Mediterranean. Mar. Geol. 195, 263–276.

Donda, F., Forlin, E., Gordini, E., Panieri, G., Buenz, S., Volpi, V., Civile, D., De Santis, L., 2015. Deep-sourced gas seepage and methane-derived carbonates in the Northern Adriatic Sea. Basin Res. 27 (4), 531–545.

Etiope, G., 2015. Natural Gas Seepage: the Earth's Hydrocarbon Degassing. https://doi.org/10.1007/978-3-319-14601-0.

Fedorik, J., Toscani, G., Lodolo, E., Civile, D., Bonini, L., Seno, S., 2018. Structural analysis and miocene-to-present tectonic evolution of a lithospheric-scale, transcurrent lineament: the Sciacca Fault (Sicilian Channel, Central Mediterranean Sea). Tectonophysics 722, 342–355.

Ferranti, L., Pepe, F., Barreca, G., Meccariello, M., Monaco, C., 2019. Multi-temporal tectonic evolution of Capo granitola and sciacca foreland transcurrent faults (sicily channel). Tectonophysics 765, 187–204 doi: 10.1016/j.tecto.2019.05. 002.

Finetti, I.R., Del Ben, A., 2005. Crustal tectono-stratigraphic setting of the Pelagian foreland from new CROP seismic data. In: Finetti, I.R. (Ed.), CROP Project: Deep Seismic Exploration of the Central Mediterranean and Italy. Elsevier, Amsterdam, pp. 581–595.

Fink, P., Zimmer, W., Punch, S., 2012. A mediterranean petroleum province on the north africa plate margin: the sicily channel. Lead. Edge 31, 794–801. https://doi.org/10.1190/tle31070794.1.

Ghisetti, F.C., Gorman, A.R., Grasso, M., Vezzani, L., 2009. Imprint of foreland structure on the deformation of a thrust sheet: the Plio-Pleistocene Gela Nappe (southern Sicily, Italy). Tectonics 28 (4). https://doi.org/10.1029/2008TC002385.

Goes, S., Giardini, D., Jenny, S., Hollenstein, C., Kahle, H.-G., Geiger, A., 2004. A recent reorganization in the south-central Mediterranean, Earth Planet. Sci. Lett. 226, 335–345. https://doi.org/10.1016/j.epsl.2004.07.038.

Granath, J.W., Casero, P., 2004. Tectonic setting of the petroleum systems of Sicily. In: Swennen, R., Roure, F., Granath, J.W. (Eds.), Deformation, Fluid Flow, and Reservoir Appraisal in Foreland Fold and Thrust Belts: AAPG Hedberg Series, pp. 391–411 no. 1.

Gueguen, E., Doglioni, C., Fernandez, M., 1998. On the post-25 Ma geodynamic evolution of the western Mediterranean. Tectonophysics 298, 259–269.

Ho, S., Imbert, P., Hovland, M., Wetzel, A., Blouet, J.-P., Carruthers, D., 2018. Downslope-shifting pockmarks: interplay between hydrocarbon leakage, sedimentation, currents and slopes topography. Int. J. Earth Sci. 107, 2907–2929.

Hovland, M., Sommerville, J., 1985. Characteristics of two natural gas seepages in the North Sea. Mar. Petrol. Geol. 2, 319–326. https://doi.org/10.1016/0264-8172(85)90027-3.

Hovland, M., Judd, A.G., Burke, R., 1993. The global flux of methane from shallow submarine sediments. Chemosphere 26, 559–578.

Huuse, M., Jackson, C.A.-L., Rensbergen, P.V., Davies, R.J., Flemings, P.B., Dixon, R.J., 2010. Subsurface sediment remobilization and fluid flow in sedimentary basins: an overview. Basin Res. 22 (4), 342–360.

Jenner, E., 2002. Azimuthal AVO: methodology and data examples. Lead. Edge 21 (8), 713–808. https://doi.org/10.1190/1.1503184.

Jongsma, D., Van Hinte, J.E., Woodside, J.M., 1985. Geologic structure and neotectonics of the North African continental margin south of Sicily. Mar. Petrol. Geol. 2, 156–179.

Judd, A., Davies, G., Wilson, J., Holmes, R., Baron, G., Bryden, I., 1997. Contributions to atmospheric methane by natural seepages on the UK continental shelf. Mar. Geol. 137 (1–2), 165–189.

Judd, A.G., Hovland, M., 1992. The evidence of shallow gas in marine sediments. Continent. Shelf Res. 12, 1081–1095. https://doi.org/10.1016/0278-4343(92)90070-Z.

Judd, A.G., Hovland, M., Dimitrov, L.I., Garcia Gil, S., Jukes, V., 2002. The geological methane budget at continental margins and its influence on climate change. Geofluids 2, 109–126.

Kumar, P.C., Alves, T., Sain, K., 2021. Submarine canyon systems fusing the migration of sub-surface fluid in the Canterbury Basin, South Island, New Zealand. Sci. Rep. 11 (1), 1–16.

Li, Y., Downtown, J., Xu, Y., 2007. Practical aspects of AVO modeling. The Leading Edge 26 (3), 295–311. https://doi.org/10.1190/1.2715053.

Lodolo, E., Civile, D., Zecchin, M., Zampa, L., Accaino, F., 2019. A series of volcanic edifices discovered a few kilometers off the coast of SW Sicily. Mar. Geol. 416 https://doi.org/10.1016/j.margeo.2019.105999.

Lodolo, E., Renzulli, A., Cerrano, C., Calcinai, B., Civile, D., Quarta, G., Calcagnile, L., 2021. Unraveling past submarine eruptions by dating lapilli tuff-encrusting coralligenous (Actea Volcano, NW Sicilian Channel). Front. Earth Sci. 9. https://ui.adsabs.harvard.edu/link_gateway/2021FrEaS...9..293L/doi:10.3389/feart.2021.664591.

Løseth, H., Gading, M., Wensaas, L., 2009. Hydrocarbon leakage interpreted on seismic data. Mar. Petrol. Geol. 26.

Mancuso, M.R., Catalano, R., 2020. Evidenze sismostratigrafiche di fenomeni da espulsione di fluidi, superficiali e profondi, nell'offshore tra Sciacca e Agrigento (Sicilia meridionale). Mem. Descr. Carta Geol. d'It. 105, 97–102.

Micallef, A., Berndt, C., Debono, G., 2011. Fluid flow systems of the Malta plateau, central Mediterranean Sea. Mar. Geol. 284, 74–85.

Palano, M., Ursino, A., Spampinato, S., Sparacino, F., Polonia, A., Gasperini, L., 2020. Crustal deformation, active tectonics and seismic potential in the Sicily Channel (Central Mediterranean), along the Nubia–Eurasia plate boundary. Sci. Rep. 10 https://doi.org/10.1038/s41598-020-78063-1.

Parello, F., Allard, P., D'Alessandro, W., Federico, C., Jean-Baptiste, P., Catani, O., 2000. Isotope geochemistry of Pantelleria volcanic fluids, Sicily Channel rift: a mantle volatile end-member for volcanism in southern Europe. Earth Planet Sci. Lett. 180, 325–339.

Reuther, C.D., Ben-Avraham, Z., Grasso, M., 1993. Origin and role of major strike-slip transfers during plate collision in the central Mediterranean. Terra. Nova 5 (3), 249–257.

Riva, A., Pace, P., Di Cuia, R., Fink, P., 2017. Re-evaluating the Nilde oilfield (offshore sicily): a miocene carbonate reservoir in a submerged central mediterranean thrust belt. In: AAPG Regional Conference 2017. Larnaca, Cyprus.

Savini, A., Malinverno, E., Etiope, G., Tessarolo, C., Corselli, C., 2009. Shallow seep-related seafloor features along the Malta Plateau (Sicily channel – Mediterranean Sea): morphologies and geo-environmental control of their distribution. Mar. Petrol. Geol. 26, 1831–1848.

Schroot, B., Schüttenhelm, R., 2003. Shallow gas and gas seepage: expressions on seismic and other acoustic data from The Netherlands North Sea. J. Geochem. Explor. 78, 305–309. https://doi.org/10.1016/S0375-6742(03)00112-2.

Shuey, R.T., 1985. A simplification of the Zoeppritz equations. Geophysics 50 (4), 609–614.

Siddall, M., Rohling, E.J., Almogi-Labin, A., Hemleben, C., Meischner, D., Schmelzer, I., Smeed, D.A., 2003. Sea-level fluctuations during the last glacial cycle. Nature 423, 853–858.

Soumaya, A., Ben Ayed, N., Delvaux, D., Ghanmi, M., 2015. Spatial variation of present day stress field and tectonic regime in Tunisia and surroundings from formal inversion of focal mechanisms: geodynamic implications for central Mediterranean. Tectonics 34, 1154–1180.

Spatola, D., Micallef, A., Sulli, A., Basilone, L., Ferreri, R., Basilone, G., Bonanno, A., Pulizzi, M., Mangano, S., 2018. The Graham Bank (sicily channel, central Mediterranean Sea): seafloor signatures of volcanic and tectonic controls. Geomorphology 318. https://doi.org/10.1016/j.geomorph.2018.07.006.

Taner, M.T., Koehler, F., Sheriff, R.E., 1979. Complex seismic trace analysis. Geophysics 44 (6), 1041–1063. https://doi.org/10.1190/1.1440994.

Taviani, M., Angeletti, L., Ceregato, A., Foglini, F., Froglia, C., Trincardi, F., 2013. The Gela Basin pockmark field in the strait of Sicily (Mediterranean Sea): chemosymbiotic faunal and carbonate signatures of postglacial to modern cold seepage. Biogeosci. Discuss. 10, 967–1009. https://doi.org/10.5194/bgd-10-967-2013.

Vesnaver, A., Böhm, G., 2000. Staggered or adapted grids for seismic tomography? Lead. Edge 19 (9), 944–950.

Vesnaver, A., Böhm, G., Galuppo, P., 1999. Staggered versus adapted grids for the joint 3D inversion of surface and well data. In: 69th Annual Internat. Mtg., Soc. Expl. Geophys. Expanded Abstracts, Houston, pp. 1793–1796.

Washington, H.S., 1909. The submarine eruption of 1831 and 1891 near Pantelleria. Am. J. Sci. 27, 31–50.

Wessel, P., Smith H.F., W., 1991. Free software helps map and display data. Eos Trans. Am. Geophys. Union 72 (41), 445–446. https://doi.org/10.1029/90EO00319.

Yilmaz, O., 2001. Seismic Data Analysis, second ed. SEG.

Zoeppritz, K., 1919. Erdbebenwellen VIII B, Über Reflexion ad Durchgang seismischer wellen durch Unstetigkeitsflachen: Göttinger Nach, pp. 66–84.